

Accepted Manuscript

Crystalline Hydroxyapatite Thin Films Produced at Room Temperature – An Opposing Radio Frequency Magnetron Sputtering Approach

Zhendong Hong, Lan Luan, Se-Bum Paik, Bin Deng, Donald E. Ellis, John B. Ketterson, Alexandre Mello, Jean G. Eon, Joice Terra, Alexandre Rossi

PII: S0040-6090(07)00230-1
DOI: doi: [10.1016/j.tsf.2007.02.089](https://doi.org/10.1016/j.tsf.2007.02.089)
Reference: TSF 22862

To appear in: *Thin Solid Films*

Received date: 11 July 2006
Revised date: 28 December 2006
Accepted date: 7 February 2007



Please cite this article as: Zhendong Hong, Lan Luan, Se-Bum Paik, Bin Deng, Donald E. Ellis, John B. Ketterson, Alexandre Mello, Jean G. Eon, Joice Terra, Alexandre Rossi, Crystalline Hydroxyapatite Thin Films Produced at Room Temperature – An Opposing Radio Frequency Magnetron Sputtering Approach, *Thin Solid Films* (2007), doi: [10.1016/j.tsf.2007.02.089](https://doi.org/10.1016/j.tsf.2007.02.089)

This is a PDF file of an unedited manuscript that has been accepted for publication. As a service to our customers we are providing this early version of the manuscript. The manuscript will undergo copyediting, typesetting, and review of the resulting proof before it is published in its final form. Please note that during the production process errors may be discovered which could affect the content, and all legal disclaimers that apply to the journal pertain.

Crystalline Hydroxyapatite Thin Films Produced at Room Temperature – An Opposing Radio Frequency Magnetron Sputtering Approach

Zhendong Hong^{a,1,*}, Lan Luan^a, Se-Bum Paik^a, Bin Deng^{a,b}, Donald E. Ellis^{a,b}, and John
B. Ketterson^a

^aDepartment of Physics and Astronomy, Northwestern University, Evanston, Illinois
60208, USA

^bDepartment of Chemistry, Northwestern University, Evanston, Illinois 60208, USA
and

Alexandre Mello^{c,d}, Jean G. Eon^e, Joice Terra^c and Alexandre Rossi^c

^cCentro Brasileiro de Pesquisas Físicas, Rio de Janeiro, RJ 22290, Brasil

^dInstituto Militar de Engenharia, Rio de Janeiro, RJ 22290, Brasil

^eInstituto de Química, Universidade Federal do Rio de Janeiro RJ 21949, Brasil

¹hong@northwestern.edu

Abstract

Hydroxyapatite (HA) films have been widely recognized for their biocompatibility and utility in promoting biointegration of implants in both osseous and soft tissue. Conventional sputtering techniques have shown some advantages over the commercially available plasma spraying method; however, the as-sputtered films are usually amorphous which can cause some serious adhesion problems when post-deposition heat treatment is necessitated. In this paper we present an opposing radio frequency (RF) magnetron sputtering approach for the preparation of HA thin films on various substrates at low power levels. Using this alternative RF magnetron geometry, as-sputtered HA films are nearly stoichiometric, highly crystalline, and strongly bound to the substrate.

Post deposition heat treatment under 800 °C did not result in a marked improvement in the degree of crystallinity of the films. In addition, dissolution experiments show that as-sputtered films are more stable than annealed ones. As-sputtered films grown on amorphous silica substrates exhibit X-ray diffraction (XRD) patterns similar to those of randomly orientated HA powder. On the other hand, films deposited on oriented substrates such as Si(100) and Si(111) show a polycrystalline HA XRD pattern but with some strongly preferred orientations, indicating that HA crystallization is sensitive to the nature of the substrate. The results suggest that the opposing RF magnetron sputtering approach has some potential to produce high quality HA films on metallic implants.

Keywords: Hydroxyapatite; Thin films; RF opposing magnetron sputtering; Off-axis sputtering; Heat treatment

1. Introduction

Hydroxyapatite (HA), with the chemical formula $\text{Ca}_{10}(\text{PO}_4)_6(\text{OH})_2$, is chemically similar to the main inorganic constituent of natural bone (bone mineral is a carbonate-containing calcium deficient hydroxyapatite). Thanks to its inherent biocompatibility synthetic HA forms a strong bond with human bone and is thus a widely used implant material. Since ceramic HA is brittle, and thus not suitable for load-bearing applications, HA films are applied to dental and medical implant materials to combine the superior mechanical properties of the implant metals with the biocompatibility of HA [1,2].

Currently the most commercially utilized technique to deposit HA is plasma spraying. Although this technique has a high deposition rate, there are some disadvantages such as a nonstoichiometric film, poor adhesion between film and substrate, etc [3,4]. Previous

studies have demonstrated that HA films made by conventional radio frequency (RF) magnetron sputtering show good biological behavior [5,6].

Almost all groups have reported that the as-sputtered HA films are amorphous [7-13]. Although a few groups reported the formation of polycrystalline HA when sputtered at high power, the deposition process is usually accompanied by the decomposition of HA into other calcium phosphate phases [14].

Unfortunately, it is also known that a high concentration of amorphous phase in the film can cause excessive dissolution in a physiological environment and consequently reduce the film integrity of the implants [15,16]. To decrease the solubility of amorphous HA films the crystallinity needs to be enhanced [17], historically making post-deposition annealing a requirement. However, annealing is time consuming, and, more important, is detrimental to the thermo-stability of the underlying implant metal and is often the main cause of crack formation and the degradation in adhesion of the film to the substrate. This effect is apparently due to the residual stress resulting from the thermal mismatch between the substrate and the HA film.

In this work we have utilized an alternative magnetron sputtering system based on a right-angle geometry to prepare thin and adherent HA films on different substrates. Our chamber is specially designed such that substrate holder can be positioned at right angles to the opposing targets. This geometry evolved out of our earlier experience in the deposition of high T_c superconducting thin films [18]. We verified that when two opposing magnetrons were placed such that their magnetic fields added, the right-angle geometry can simultaneously achieve low substrate back-sputtering and a high deposition rate. With these conditions we could produce as-sputtered HA thin films with desirable

stoichiometry and crystallinity. The influence of the substrate orientation on HA crystal growth was also investigated in this work. For this we prepared HA films on amorphous substrates such as fused silica and oriented substrates such as silicon single crystals.

2. Experimental Details

2.1 Targets and substrates preparation

Stoichiometric HA powder (Ca/P = 1.67) were synthesized from dropwise addition of an ammonium phosphate aqueous solution to a calcium phosphate solution at 90 °C and pH=11. The precipitate was separated by filtration, repeatedly washed with boiling deionized water and dried at 100 °C for 24 hours. The powder was manually ground and particles were separated by sieving. Cylindrical tablets with a diameter of 38 mm and variable heights were prepared by uniaxially pressing HA under 30 MPa. Targets with 25 mm in diameter were then prepared by sintering tablets at 1100 °C for 2 hours.

The substrates we experimented included fused silica (Precision Glass & Optics, CA), single crystal (001) & (111) silicon wafers (Virginia Semiconductor, VA), and single crystal (111) MgO (MTI, CA). All substrates were ultrasonically cleaned with acetone before deposition. In addition, the silicon substrates were etched in 5% hydrofluoric acid for 5 minutes to remove the surface oxide layer and then rinsed with water, leaving a hydrogen-terminated surface that is stable against oxidation under ambient conditions for a short period of time [19].

2.2 Opposing magnetron sputtering system and film deposition

The block diagram of the custom-built, opposing magnetron, sputtering system is shown in Fig. 1. The two water cooled sputtering guns were fabricated in-house from standard copper tubing, an epoxy insulating section, and two quick-connect vacuum feed-throughs; the guns attach to the sputtering chamber, a commercial six-way cross with a volume of about 1L, via quick-connect vacuum flanges. The magnetic fields are provided by cylindrical NdFeB permanent magnets located inside the water-cooled electrodes on which the targets are mounted. The detachable HA targets (25 mm in diameter) are bonded to permalloy discs with silver epoxy and are held to the opposing sputtering guns by the magnetic force arising from the magnets in the guns; this approach facilitates easy mounting and removal of the targets.

The chamber was evacuated with a turbo pump, which was backed by a mechanical pump, to a base pressure lower than 10^{-6} torr. Ultra-high purity oxygen was used as the reactive gas component, combined with argon as the sputtering gas. RF power (fixed at a total of 130 watts) was applied to the two opposing targets through an impedance matching network, with the substrate holder positioned at right angles to the targets, as noted above. Residual gas species and their molar ratios were monitored and controlled with the help of a residual gas analyzer. Pre-sputtering of the targets was routinely performed when they were first pumped down. During this phase surface contaminants were removed and deposited onto a T-shaped, externally positionable, shutter placed between the targets and the substrate. This conditioning procedure was performed every time the target was exposed to the atmosphere (which contains potentially reactive components such as CO_2) for more than a brief period. In our experiments the partial pressures of argon and oxygen were set at 5.0 mtorr and 1.0 mtorr, respectively (from our

previous experience we found that this ratio yielded both a reasonable sputtering rate and approximately kept the stoichiometry of the targets). During the sputtering process the temperature of the substrate holder rose to around 60 °C due to heating from the plasma discharge. The deposition time was kept constant at 3 hours.

Two series of films were prepared under identical experimental conditions on all four substrates utilized. After deposition, one series was left as-sputtered for further characterization, while the other series was annealed at 800 °C for 3 hrs with argon and saturated water vapor (flow rate $\cong 200 \text{ mm}\cdot\text{min}^{-1}$) for comparative studies.

2.3 *Film characterization*

2.3.1 *Film thickness and surface morphology*

The substrate was held in place by a frame that was screwed in place, thus leaving a shadow-generated step on the edge of the film. The height of the step was measured with a Tencor P-10 surface profiler (KLA-Tencor, CA, USA).

To reduce the dielectric film charging problem, the surface micromorphology of both as-sputtered and annealed HA films was examined using a Variable Pressure Scanning Electron Microscope (Hitachi S-3500N VP-SEM), operating at an accelerating voltage of 30 kV. Nitrogen with partial pressure of 80 Pa was introduced into the chamber, and X-ray emission was detected by a Robinson backscattered-electron detector. Light microscopy (performed with a Nikon Epiphot optical microscope coupled with a CCD) was utilized to observe the surface morphology of the as-sputtered and annealed films, both before and after the dissolution test.

2.3.2 Crystallographic structure

A Rigaku ATX-G thin film X-ray diffractometer was used to characterize the film structure. Using Cu K_{α} radiation at 12 kW, a thin film sample was first aligned to a half-split position with narrow slits (source slit 0.1 mm \times 5 mm, guard slit 0.2 mm \times 10 mm, receiving slit 0.2 mm), and then a θ - 2θ scan was executed over a range of 9° to 60° (70° for HA/Si (111)) with wide slits (source slit 0.5 mm \times 5 mm, guard slit 0.5 mm \times 10 mm, receiving slit 0.5 mm) to increase beam intensity. The step size and scan speed were set at 0.01° and $1^{\circ}/\text{min}$, respectively. Qualitative phase identification was done by comparing the measured XRD intensities with the published International Center for Diffraction Data (ICDD) powder diffraction files.

2.3.3 Fourier transform infrared (FTIR) and Raman spectroscopy

Diffuse Reflectance Infrared Fourier Transform Spectroscopy experiments were performed using a Thermo Nicolet Nexus 870 FTIR spectrometer with the Tabletop optics module. The spectra were collected over a range of $400\sim 4000\text{ cm}^{-1}$ with a resolution of 4 cm^{-1} and averaged over 256 scans to characterize the phosphate, hydroxyl, and carbonate functional groups.

Raman spectra of the HA targets and HA films were recorded on a Raman microscope constructed from components at hand. Samples were excited by a 532 nm continuous wave Nd:YAG laser using side illumination. Raman emissions were collected by a microscope objective lens and analyzed by a single grating spectrometer equipped with a liquid nitrogen cooled CCD. The scattered excitation light was rejected by a Semrock Raman edge filter.

2.3.4 Dissolution test

There have recently been reports on the *in vitro* dissolution behavior of magnetron sputtered HA films [20-23]. As a preliminary dissolution test, our as-sputtered and annealed HA films on Si (111) were immersed in deionized water (pH=7.0) for 24 hours. This represents a more severe test compared to those experiments performed in a more typical physiological solution (such as simulated biological fluid), which contain calcium, phosphate, and other ions. Assuming the system had stabilized with respect to dissolution and precipitation during the time of the experiment, the effect of dissolution on surface morphology, chemical composition, and film structure could be characterized.

3. Results and discussion

3.1 Film thickness

All films were deposited for 3 hours at 130 watts. Irrespective of the substrate, the resulting thicknesses obtained were 5000 Å, which gave an average deposition rate of 660 Å/hr, or $120(\text{Å} / \text{hr}) / (\text{W} / \text{cm}^2)$. The film thickness and uniformity were measured using a surface profiler. In our experiments we found that under the conditions described in section 2.2, and for the chosen substrate position, the thickness was rather uniform (Fig. 2). It is possible to improve the thickness uniformity by moving the substrate farther away from the plasma region, but a tradeoff in terms of deposition rate and film purity (due to excessive gas molecule collisions) is then involved.

3.2 Film structure and phase identification

3.2.1 Fourier Transform Infrared Spectroscopy (FTIR) and Raman spectroscopy

Infrared spectra were taken for HA films on silicon (111) and (001) substrates. (Fused silica and MgO strongly absorb infrared and are thus not suitable for infrared measurements). Shown in Fig. 3 are representative infrared spectra of the HA films deposited on Si(111) and Si(001). The FTIR spectrum of the HA film on Si(111) is composed of sharp phosphate and hydroxyl absorption bands, indicating that PO_4^{3-} and OH^- sites are well ordered in film structure. The pronounced hydroxyl bands at 632 and 3572 cm^{-1} are typical of hydroxyapatite with a high degree of crystallinity, comparable to HA powder sintered at high temperature as shown in Fig. 3. The small narrow bands at 3544 cm^{-1} and 3642 cm^{-1} likely arise from OH^- at different sites. The broad bands at 1640 cm^{-1} arising from water molecules, which is always present in the FTIR spectra of powdered HA, was absent in the HA films. This result confirms that HA films are crystalline without micro porosity. The hydroxyapatite phosphate absorption bands ν_1, ν_2 and ν_4 were found at 468, 563, 596, and 964 cm^{-1} which are very close to those of a stoichiometric HA (ν_1 at 962 cm^{-1} ; ν_2 at 462 and 474 cm^{-1} ; ν_4 at 571 and 601 cm^{-1}). In the region 1000 - 1150 cm^{-1} , ν_3 bands of stoichiometric HA at 998 and 1083 cm^{-1} were identified but in the position of ν_3 components at 1046 cm^{-1} and 1032 cm^{-1} a broad band at 1025 cm^{-1} was seen. This band was identified in calcium deficient HA [24]. Bands not belonging to stoichiometric HA such as 1125 cm^{-1} could be attributed to ν_6 degenerated stretching of HPO_4^{2-} ions, which are usually found in brushite. It is also found that phosphate and hydroxyl bands of HA films on Si(111) are narrower than those of HA films on Si(001), suggesting that the former is a more crystallized and ordered structure.

All films showed carbonate bands at 1416 cm^{-1} , 1456 cm^{-1} , 1494 cm^{-1} , and 1548 cm^{-1} .

These bands are typical of carbonate occupying OH⁻¹ and PO₄³⁻ sites in HA hexagonal structure and suggests the formation of carbonated HA films. The carbonate contamination may come from adsorption and diffusion of CO₂ molecules in the air during the sputtering process and after.

Fig. 4(a) shows the Raman spectrum obtained from one of the HA targets used in these experiments. Peaks were found at 435 cm⁻¹, 588 cm⁻¹, 962 cm⁻¹, 1049 cm⁻¹, and 1080 cm⁻¹. The characteristic peak at 962 cm⁻¹ is due to symmetric stretching vibrations of the phosphate group (PO₄³⁻). The position of this peak is a good indicator of the degree of crystallinity of the material: it shifts to ~955 cm⁻¹ in more amorphous, heavily carbonated bone, but is found at ~963 cm⁻¹ in more ordered, non-carbonated bone [25]. The 962 cm⁻¹ peak of the HA target is very sharp, indicating it is well crystallized. The weak peak at 1078 cm⁻¹ can be assigned to the carbonate group (B-type carbonate, ν₃) [25,26]. Fig. 4(b) shows the Raman spectrum of the as-sputtered HA film after subtracting the Si(001) background. The major peak shifts slightly, to 958 cm⁻¹, suggesting partial crystallization of the HA film. The fact that full width at half maximum (FWHM) of this peak is broader than that of the HA target supports our conclusion.

3.2.2 X-Ray Diffraction (XRD)

HA has a hexagonal structure with the main powder diffraction peaks appearing at 2θ = 10.84°(100, 12%), 25.9°(002, 40%), 28.9°(210, 18%), 31.8°(211, 100%), 32.2°(112, 60%), 32.9°(300, 60%), and 34.0°(202, 25%) (according to ICDD PDF # 00-009-0432). Shown in Fig. 5 are the X-ray diffraction patterns of as-synthesized HA powder, HA powder annealed at 1100 °C and as-sputtered films deposited for 3 hours on SiO₂, MgO,

and Si(001). The main HA peaks are observed in the XRD patterns of the as-sputtered films, reinforcing the FTIR results which reveal that the films are mainly composed of HA. The XRD patterns of the as-sputtered films show sharp peaks like those of sintered HA powder, indicating that as-sputtered HA films have high crystallinity. Although the XRD patterns are typical of a polycrystalline material, some texturing, or equivalently a tendency toward preferred orientations, was observed. Differences in crystallinity and texturing were observed in as-sputtered HA films because relative peak intensity and line-width depended on the substrate used. Films deposited on amorphous SiO₂ showed a poorly resolved diffraction pattern with broader peaks than those observed on films deposited on Si(111) and Si(001). No preferred orientation was observed in films deposited on silica. The crystallite size broadening of a diffraction peak can be related to the mean crystallite size via the Scherer equation $\left(t = \frac{0.9 \cdot \lambda}{B \cdot \cos \theta_B} \right)$, where t is the mean crystallite size, B is the peak line-width at half maximum (in radian), θ_B is the Bragg diffraction angle and λ is the X-ray (CuK α radiation in our case) wavelength. The (002) and (300) reflections were chosen for analysis of the broadening of the Bragg line, the Gaussian symmetrical profile function was fitted to the two Bragg peaks for extraction of FWHM. The mean crystallite size was then estimated to be within the range of 50 to 100 nm and the results were quite consistent with each other when computing from different diffraction peaks.

It was found (Table 1) that the intensity ratio between the (002) and (300) diffraction peaks of HA films deposited on all substrates are markedly larger than that of standard HA powder. This result shows that crystallization along (002) planes is more preferred in

HA films than in HA powder precipitated in aqueous solution, independent of the substrate orientation.

As for the as-sputtered film on fused silica and MgO(111), a polycrystalline HA phase was observed as well, however, no preferred orientation was observed. Instead, the resulting XRD pattern looked similar to that of the randomly orientated powder. It now seems to be clear that the (00k) crystallographic plane is the preferred growth plane for silicon single crystal substrates, while for MgO substrates this is not the case.

3.3 Influence of Thermal treatment on film characteristics

XRD analyses show that after annealing, all the films deposited on oriented substrates showed some further evolution in the degree of texture. Fig. 6 illustrates the representative powder X-ray diffraction patterns of as-sputtered and annealed HA films on Si(111) after removal of the background. It was observed that XRD patterns of annealed films are composed of sharper peaks than the as sputtered ones, which was attributed to a slight improvement in film crystallinity due to thermal treatment. However, the relative intensity of peaks along (211), (112), (300) and (002) directions become closer to the ones of polycrystalline hydroxyapatite (100%, 60%, 60% and 25%) suggesting that film preferential orientation is lost with the thermal treatment. One example is the intensity ratio between (002) and (300) peaks of the as-sputtered film deposited on Si(111) changed from 1.64 to 0.79 after annealing at 800°C. The latter value is closer to 0.67 which is found in stoichiometric HA powder. Also, the large value of the (002) to (300) peak intensity ratio showed that films deposited on amorphous SiO₂ substrate also have a preferential growth along c axis. However, thermal annealing didn't

change the film texture as observed in those films deposited on oriented substrates.

The annealed silica films showed a polycrystalline XRD patterns as the as-sputtered films. After post deposition annealing, the (h00) peaks increased dramatically, while the main powder diffraction peaks, (211) and (112), dropped in intensity.

Fig. 7a-b shows the comparison of surface morphology of as-sputtered and annealed HA films on fused SiO₂. It was observed that the as-sputtered HA film was very smooth with a few sporadic HA particulates. In contrast, a post deposition heat treatment at 800 °C in the argon/water-vapor environment roughened the surface and resulted in severe crack formation, apparently due to the thermal mismatch between film and the SiO₂ substrate.

An interesting behavior was found in films grown on oriented substrate like Si(001) (Fig. 7c-d): the as-sputtered film surface was still rather smooth and featureless; however, after annealing under the conditions described above the film surface collapsed into a porous pattern spread out over the whole substrate surface.

3.4. Film dissolution behavior

After immersing in deionized water for 24 hours, the as-sputtered and annealed HA films on Si(111) were taken out for X-ray diffraction measurements. It was found that the XRD pattern of the as-sputtered film was almost identical as before, whereas the diffraction peak intensity of the annealed sample dropped to the background noise level (Fig. 8). This result supports our earlier observations that as-sputtered films are less soluble and more stable than annealed ones. Optical microscopy was used to inspect the change in surface macro-morphology of the as-sputtered and annealed HA films on Si(111) after the dissolution test as shown in Fig. 9. It was found that only a fraction of

the as-sputtered film had been dissolved. A more detailed examination revealed the appearance of Newton rings, which is evidence that an air gap has formed between the film and the substrate; it is also interesting that the dissolution process occurs in a nearly circularly-symmetric manner. In contrast, the annealed film suffered great damage and only sporadic particulates remained. This indicates that our as-sputtered films are less soluble, possibly due to a higher degree of crystallinity and better adhesion as suggested by XRD results.

4. Conclusions

An opposing magnetron sputtering system with a right angle geometry has been shown to produce textured HA thin films without the need for *in-situ* or *ex-situ* annealing. The as-sputtered films have approximately the same degree of crystallinity as that of the annealed ones, but have some advantages over the annealed ones, such as better adhesion, less surface roughness and less solubility. Our experimental results suggest that with our sputtering geometry, and under our chosen experimental conditions, HA crystallization can be realized at a low surface-energy threshold without the decomposition occurring when using high power. We have observed that different substrate orientations have great influence on film texture and structure. By adjusting the experimental conditions we could control the degree of crystallinity and, to some extent, the preferred orientations of the HA films. In summary, these results suggest that magnetron sputtering technique with a right angle geometry may be a promising alternative to plasma spray technique for film HA films on metallic implants.

Acknowledgements:

This work is supported by the National Science Foundation under grant DMR-0303491 and through CNPq. This work made use of facilities supported by the MRSEC program of the National Science Foundation (DMR-0076097) through the Materials Research Center of Northwestern University.

References

- [1] J.E.Lemons, Clin. Orthop. Rel. Res. 235 (1988) 220.
- [2] F.W.Cooke, Clin. Orthop. Rel. Res. 276 (1992) 135.
- [3] J.L.Xu, K.A.Khor, Y.W.Gu, R.Kumar, P.Cheang, Biomaterials 26 (2005) 2197.
- [4] M.J.Filiaggi, N.A.Coombs, R.M.Pilliar, J. Biomed. Mater. Res. 25 (1991) 1211.
- [5] J.A.Jansen, J.G.C.Wolke, S.Swann, J.P.van der Waerden, K.de Groot, Clin. Oral Implant Res. 4 (1993) 28.
- [6] J.E.G.Hulshoff, K.van Dijk, J.P.van der Waerden, J.G.C.Wolke, L.A.Ginsel, J.A. Jansen, J. Biomed. Mater. Res. 29 (1995) 967.
- [7] K.van Dijk, H.G.Schaeken, J.G.C.Wolke, J.A.Jansen, Biomaterials 17 (1996) 405.
- [8] J.L.Ong, L.C.Lucas, Biomaterials 15 (1994) 337.
- [9] K.Yamashita, T.Arashi, K.Kitagaki, S.Yamada, T.Umegaki, J. Am. Ceram. Soc. 77 (1994) 2401.
- [10] Y.Yang, K.Kim, C.M.Agrawal, J.L.Ong, Biomaterials 24(2003) 5131.
- [11] Y.Yang, K.H.Kim, C.M.Agrawal, J.L.Ong, J. Dent. Res. 82(2003) 833.
- [12] E.S.Thian, J.Huang, S.M.Best, Z.H.Barber, W.Bonfield, Biomaterials 26(2005) 2947.

- [13] J.G.C.Wolke, K.de Groot, J.A.Jansen, J. Biomed. Mater. Res. 39(1998) 524.
- [14] V.Nelea, C.Morosanu, M.Iliescu, I.N.Mihailescu, Appl. Surf. Sci. 228(2004) 346.
- [15] T.W.Bauer, R.C.T.Geesink, R.Zimmerman, J.T.MaMahon, J. Bone. Jt. Surg. 73A(1991) 1439.
- [16] J.P.Collier, V.A.Surprenant, M.B.Mayor, M.Wrona, R.E.Jensen, H.P.Surprenant, J. Arthrop. 8(1993) 389.
- [17] R.Z.LeGeros, Clin. Mater. 14(1993) 65.
- [18] J.Q.Zheng, M.C.Shih, X.K.Wang, S.Williams, P.Dutta, R.P.H.Chang, J.B.Ketterson, J. Vac. Sci. Technol. A 9(1991) 128.
- [19] Z.J.Cui, C.G.Takoudis, J. Electrochem. Soc. 150(2003) 694.
- [20] J.L.Ong, G.N.Raikar, T.M.Smoot, Biomaterials 18(1997) 1271.
- [21] J.G.C.Wolke, K.de Groot, J.A.Jansen, J. Mater. Sci. Mater. Med. 33(1998) 3371.
- [22] E.M.Burke, J.D.Haman, J.J.Weimer, A.B.Cheney, J.M.Rigsbee, L.C.Lucas, J. Biomed. Mater. Res. 57(2001) 41.
- [23] R.Z. LeGeros, Clin. Mater. 14(1993) 65.
- [24] E.P.Paschalis, E.DiCarlo, F.Betts, P.Sherman, R.Mendelsohn, A.L.Boskey, Calcif. Tissue Int. 59(1996) 480.
- [25] M.D.Morris, A.Carden, R.M.Rajachar, D.H.Kohn, Proc. SPIE 4614(2002) 47.
- [26] G. Leroy, G.Penel, N.Leroy, E.Bres, Appl. Spectrosc. 56(2002) 1030.

List of Figure and Table Captions

Fig. 1. Schematic of the opposing magnetron sputtering system.

Fig. 2. Thickness profile of the as-sputtered HA thin film on Si(001).

Fig. 3. FTIR spectra of sintered HA powder, as-sputtered HA thin films on Si(001) and

Si(111) substrates.

Fig. 4. Raman spectra of the (a) HA target and (b) as-sputtered HA thin film on Si (001).

Fig. 5. X-ray diffraction patterns of (a) as-synthesized HA powder, (b) HA powder annealed at 1100 °C; (c), (d) and (e) show as-sputtered films deposited for 3 hours on SiO₂, MgO, and Si(001) respectively.

Fig. 6. X-ray diffraction patterns of the as-sputtered and annealed HA thin films on Si(111) substrates.

Fig. 7. SEM micrographs of the (a) as-sputtered and (b) annealed HA films on SiO₂; Crack formation due to annealing is shown. (c) as-sputtered and (d) annealed HA thin films on Si(001). Film surface collapsed into a porous pattern spread out over the whole substrate surface.

Fig. 8. X-ray diffraction patterns of the (a) as-sputtered and (b) annealed HA films on Si(111) after dissolution test.

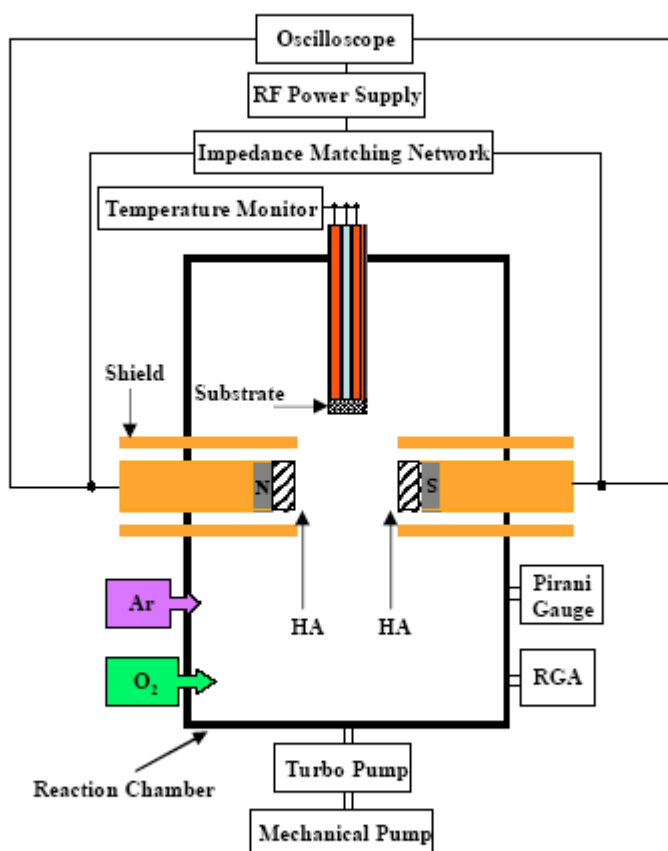
Fig. 9. Optical images of the (a) as-sputtered and (b) annealed HA films on Si (001) after dissolution test.

Table 1. Intensity ratio between (002) and (300) diffraction peaks of HA films.

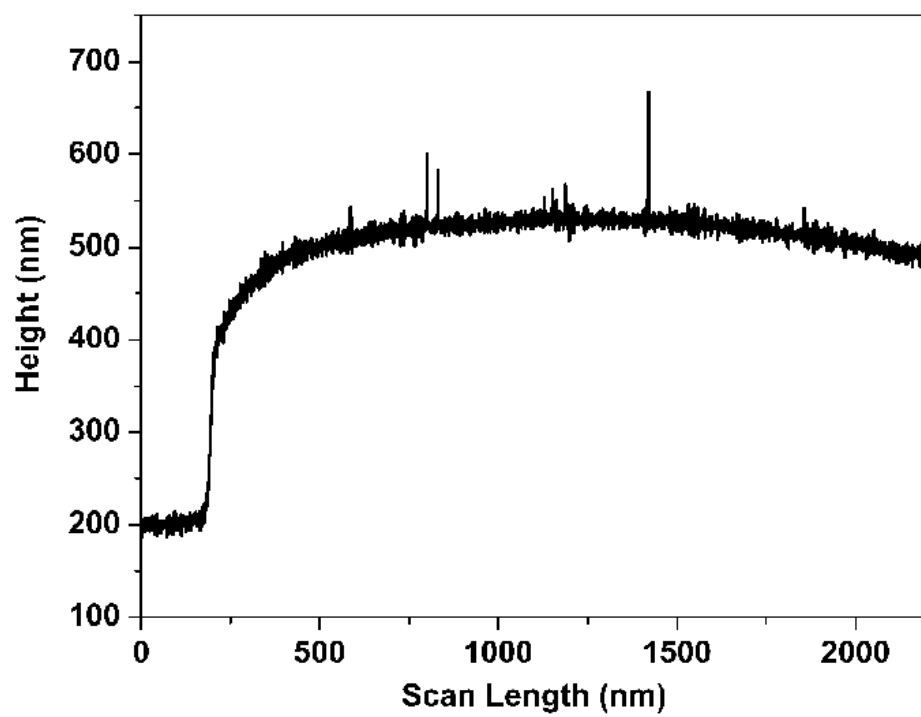
Table 1.

| Substrate material | As-sputtered | Annealed |
|---|--------------|----------|
| Intensity ratio of HA(002) to HA(300) | | |
| Si(001) | 1.29 | 0.50 |
| Si(111) | 1.64 | 0.79 |
| SiO ₂ | 1.58 | 0.54 |
| HA powder | 0.67 | 0.25 |

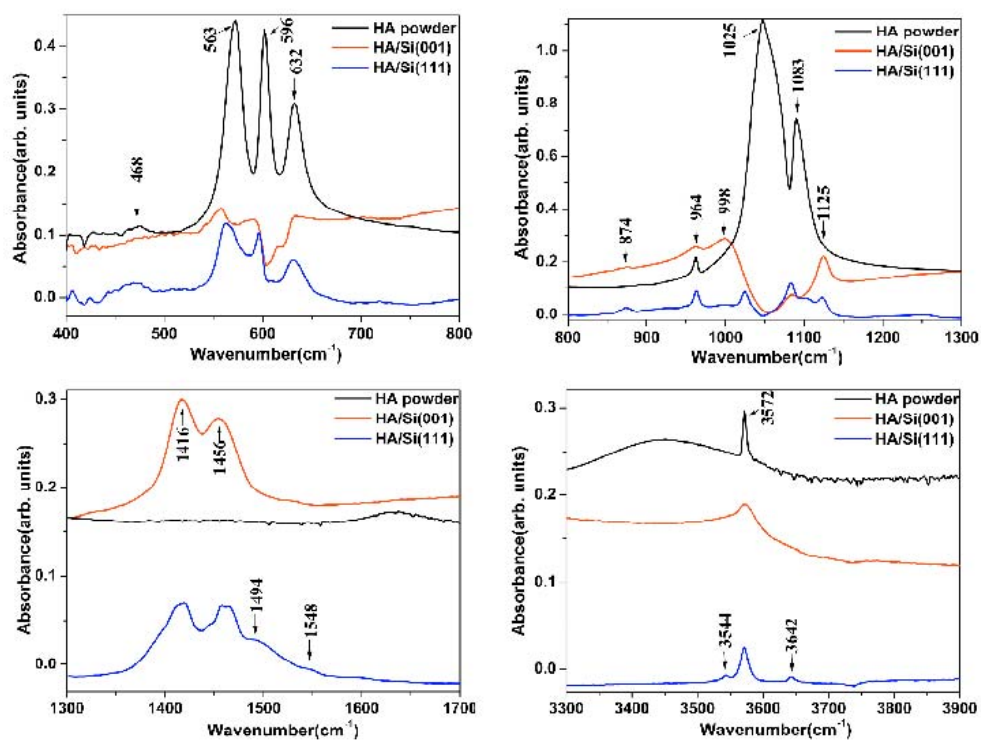
CRIP



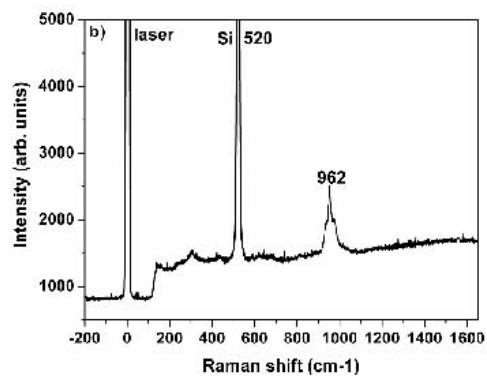
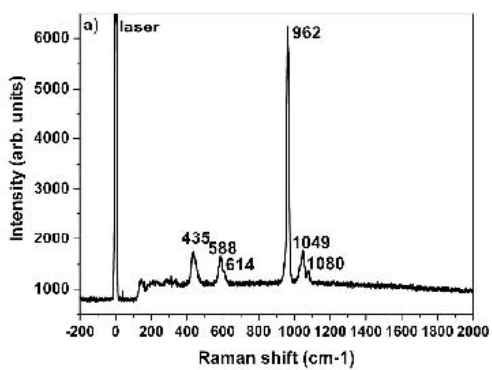
USCRIPT

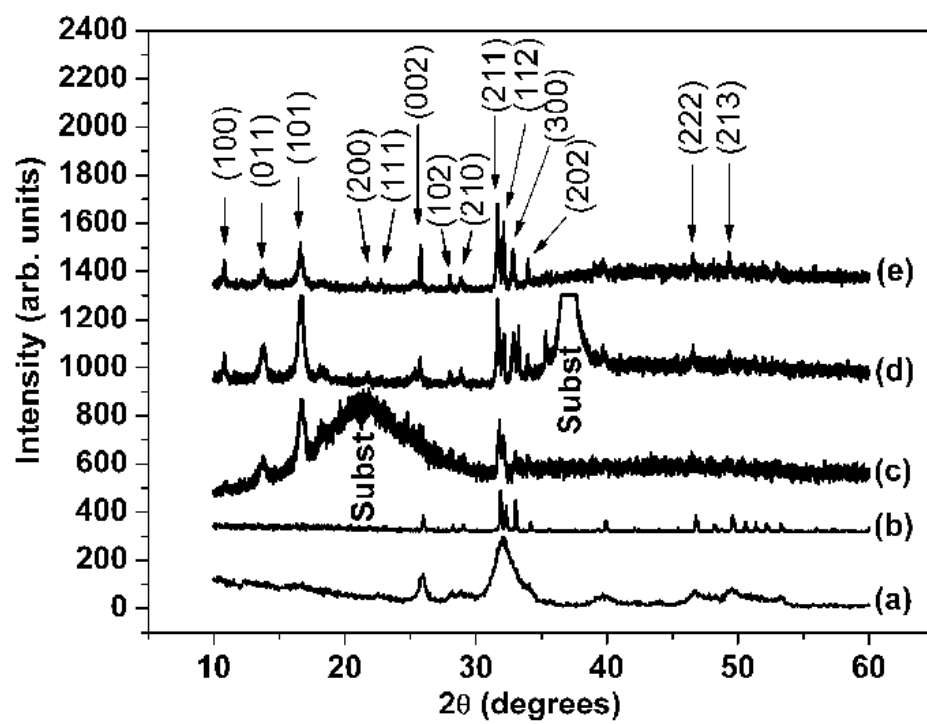


MANUSCRIPT

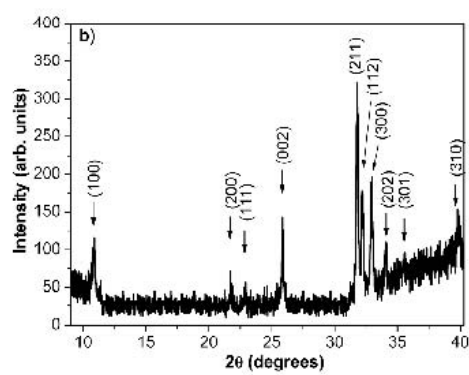
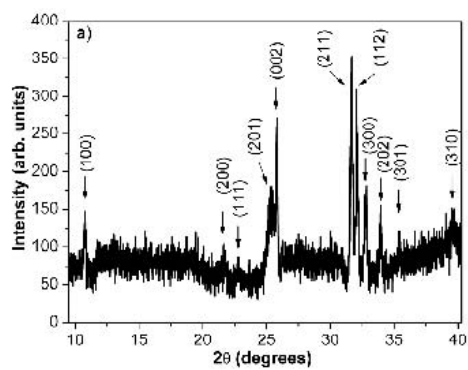


SCRIPT

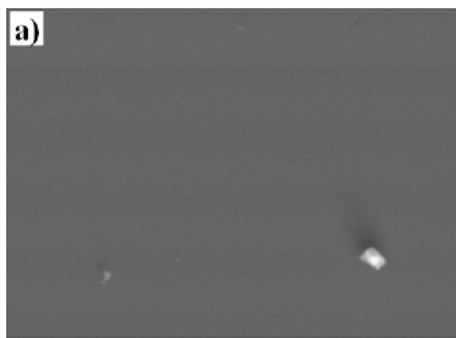
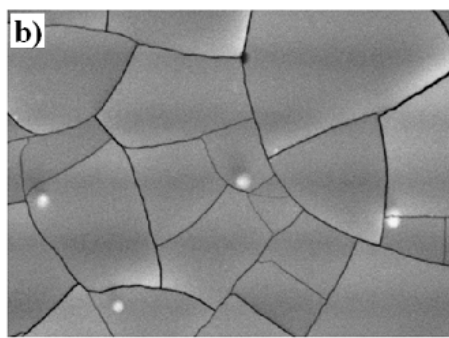
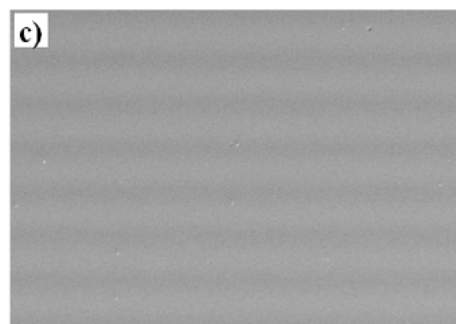
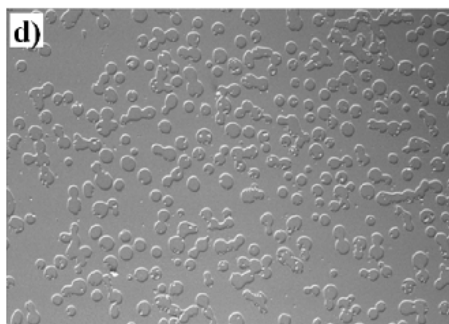




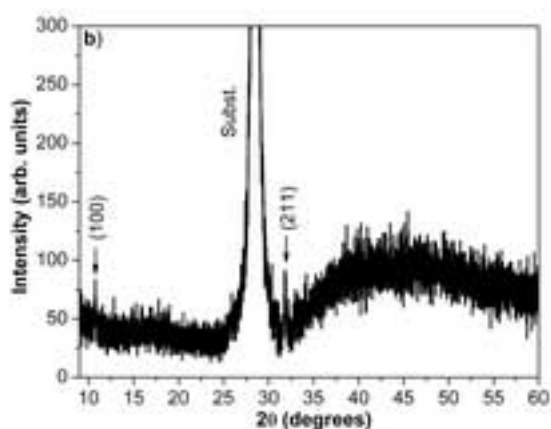
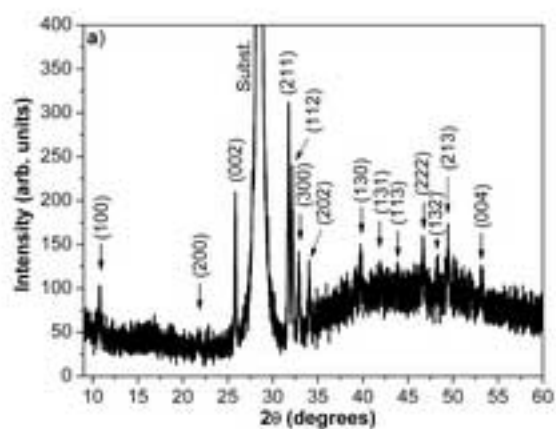
SCRIPT



SCRIPT

10 μm 5 μm 20 μm 80 μm 

ACCEPTED MANUSCRIPT



MANUSCRIPT

